Catalysis Letters (2024) 154:430–447
https://doi.org/10.1007/s10562-023-04315-0

The Effect of Lithium on NiMo/Al_2O_3 Hydrotreating Catalysts Prepared from Heteropolycompounds

Luděk Kaluža[1] · Květa Jirátová[1] · Alla A. Spojakina[2] · Jana Balabánová[1] · Dana Gulková[1] · Martin Koštejn[1] · Radostina Palcheva[2] · Georgi Tyuliev[2] · Radek Fajgar[1]

Received: 7 December 2022 / Accepted: 24 February 2023 / Published online: 17 March 2023

Abstract

Recently, simultaneous hydrotreatment of various petroleum fractions and plant feedstocks has been in demand. NiMo catalysts can be active in these processes. Therefore, supported NiMo oxide catalysts were prepared by impregnating an alumina support with Anderson's molybdenum salt (ammonium salt of nickel heteropolymolybdate $(NH_4)_4NiMo_6O_{24}H_6$) and lithium carbonate. The prepared catalysts were tested in hydrodesulfurization (HDS) of thiophene and parallel HDS/HDO (hydrodeoxygenation) of 1-benzothiophene and octanoic acid. Experimental data showed a positive effect of lithium on the parallel HDS/HDO reactions and a negative effect on the HDS of thiophene. A significant effect of lithium on the acidity and reducibility of the NiMo/Al_2O_3 catalyst as well as the contribution of an Anderson-type heteropolycompound was demonstrated.

Graphical Abstract

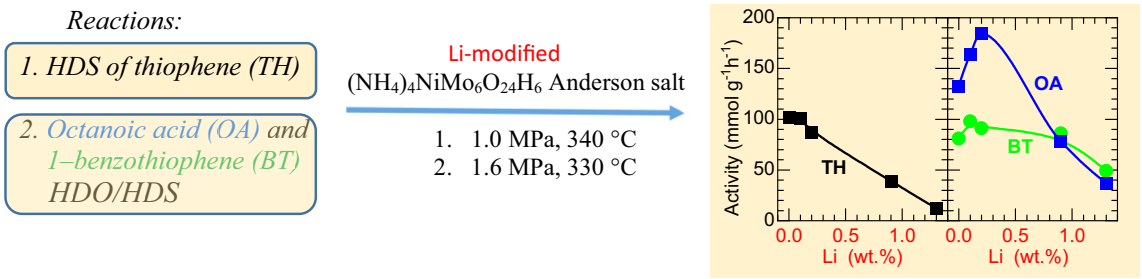

Keywords NiMo/Al_2O_3 catalysts · Lithium · Nickel heteropolymolybdate · Thiophene · 1-Benzothiophene · Octanoic acid

✉ Květa Jirátová
jiratova@icpf.cas.cz

Luděk Kaluža
kaluza@icpf.cas.cz

Alla A. Spojakina
mariamaleva@yahoo.com

Jana Balabánová
balabanova@icpf.cas.cz

Dana Gulková
gulkova@icpf.cas.cz

Martin Koštejn
Kostejn@icpf.cas.cz

Radostina Palcheva
radost@ic.bas.bg

Georgi Tyuliev
tyuliev@gmail.com

Radek Fajgar
fajgar@icpf.cas.cz

[1] Institute of Chemical Process Fundamentals of the Czech Academy of Sciences, Rozvojová 135, 165 00 Praha 6, Czech Republic

[2] Institute of Catalysis of the BAS, Akad. G. Bonchev Str., Bl. 11, 1113 Sofia, Bulgaria

1 Introduction

Hydrotreatment of different feeds for the production of fuels includes several processes such as hydrodesulfurization (HDS), hydronitrogenation (HDN), hydrogenation (HYD), hydrodemetallization (HDMe) and hydrodeoxygenation (HDO). All these reactions take place in the presence of catalysts containing either Mo or W compounds, promoted by Co and/or Ni compounds, which are supported mostly on Al_2O_3. In addition to the traditional chemical compounds used for the preparation of HDS catalysts, such as ammonium heptamolybdate, phosphomolybdic acid, nickel or cobalt nitrates, other compounds such as polyoxometalates (POMs) may be of interest due to their unique acidic properties and oxidative abilities, which can be systematically controlled by changing the countercation and the element in the anion.

Polyoxometalates (POM) are used either as a starting material for the preparation of metal oxide catalysts or directly as active components of supported catalysts. Recently, considerable attention has been paid to catalysts synthesized using polyoxometalates and various supports (Al_2O_3, TiO_2, MgO, zeolites etc.). Polyoxometalates serve as catalysts or precursors of catalysts [1, 2] acting in various acid and oxidation–reduction reactions including hydrodesulfurization (HDS).

Studies on supported polyoxometalates are particularly important because the interaction of the support and POM can alter properties of the resulting solids. The strength of the interaction can be influenced by the components of the polyoxometalates and the acid–base properties of the support. The design of the catalyst at the molecular level can be straightforward and therefore it is worth studying the properties of POM. However, there is no uniform opinion in the literature on the stability of polyoxometalates formed at the support surface [3–5].

In our previous papers on hydrodesulfurization catalysts, we have investigated the properties of Mo or W polyoxometalates of different structure and compositions prepared on different supports [6–8]. The catalysts prepared from POM, supported on silica and modified by lithium showed higher activity for HDS of thiophene than the non-modified ones [9]. We also showed that ammonium salts of polyoxometalates of Ni, Co and Fe of the Anderson-type based on alumina are suitable precursors of active sites in hydrodesulfurization reactions. Among the metal salts studied, the nickel-containing catalyst showed the highest activity in HDS [10]. In contrast to Keggin type of polymolybdates, Anderson type of polyoxomolybdates exhibit a planar structure which is an important factor for heteropolyanion–support interaction. This interaction produces an ordered distribution of metallic elements and their uniform deposition, which enhances the synergic effect [11, 12].

Moreover, catalysts prepared from Anderson salts exhibit good reducing and sulfidation properties, which represent an interesting alternative to traditional HDS systems [13]. Using Anderson type of polyoxometalates, Nikulshin et al. [14] investigated the effect of Co, Ni, Mn, Zn cations and morphology of nanosized transition metal sulfides in hydrodesulfurization of dibenzothiophene. Pimerzin et al. [15] summarized the effect of Cr, Mn, Fe, Co, Ni, Cu, Zn, Ga in Mo Anderson-type polyoxometalates on the activities in HDS and hydrogenation of thiophene and benzene.

The development of a wide range of catalysts for the hydrotreating of various petroleum fractions and secondary products is therefore significant. Thiophene is very often used as a model compound for HDS reactions representing the composition of light petrol. Thiophenes are sometimes used for simultaneous HDS/HDO with aromatic alcohols and furans representing pyrolyzed bio-oils [16, 17]. Recently, however, simultaneous hydrotreating of various petroleum fractions, vegetal raw materials and/or waste fatty materials has been required [18–21]. The use of Li-modified NiMo/Al_2O_3 catalysts in the hydrogenation of a model reaction mixture (representing a mixture of petroleum fractions and fatty feedstocks, namely 1-benzothiophene and octanoic acid) could reveal the influence of the different acid–base properties of the catalysts on the activity and selectivity of the reaction. Thiophene and 1-benzothiophene are known to exhibit similar reactivity during their HDS on NiMoS catalyst because of the identical reaction pathway [22, 23]. However, the similarity in the behavior of the two reactants may not hold true in the case of a set of catalysts that differ significantly in their surface properties affecting HDS reaction pathway. In addition, reaction byproducts formed during HDO of hydrocarbon feeds, high oxygen content mainly in the form of –OH or –COOH groups and their derivatives can influence the HDS reaction pathway of, e.g., 1-benzothiophene. Therefore, a mixture of 1-benzothiophene and fatty acid is a good choice for waste fats and heavier hydrocarbon fraction co-hydrotreatment focused on environmentally friendly diesel production, while a mixture of thiophene and furan will be an excellent model mixture for light hydrocarbon fraction co–hydrotreating.

Improvements in hydrocatalytic processes, including the simultaneous hydrotreating of various petroleum fractions and plant feedstocks has recently been required due to the use of new renewable feedstocks and the demand for environmentally friendly fuel production. Therefore, not only hydrodesulfurization reactions are necessary in the processing of modern feedstocks. New feeds derived from waste plastics or renewable sources introduce high oxygen content into hydrocarbon feeds up to approximately 38% by weight [24–26] (instead of approximately 2% in other feeds). When

synthetic or renewable feedstocks are co-hydrotreated with fossil-based feedstocks, sulfide hydrotreating catalysts must provide a large-scale hydrodeoxygenation reaction (HDO) in addition to the hydrodesulfurization reaction (HDS).

We found previously [27] that the NiMo sulfide phase exhibits higher HDO and HDS activity than the sulfide phase of CoMo and Mo supported on MgO, Al_2O_3, ZrO_2, TiO_2, and activated carbon. The type of support influenced the HDO/HDS selectivity and the active phase used and was the highest for NiMo/TiO_2. Varakin et al. [28] suggested double-bed catalytic system consisting of unsupported MoS_2 catalyst and a NiMo catalyst supported by Al_2O_3 for co-hydrotreating of a mixture of waste vegetable oils and oil fractions. Nikulshin et al. [18] showed that catalysts more useful for the HDO of renewable feed are those on the inert C-coated Al_2O_3 supports. However, acidity plays a major role in hydrodeoxygenation reactions and thus, seems to be crucial for HDO of fatty acids containing feeds because it affects the formation of linear or branched hydrocarbons [27, 29].

Considering the dependence of the activity of supported polyoxometalates on the composition, type of support and added compounds, an important step in tailoring catalysts for HDS/HDO reactions is the selection of active and stable polyoxometalates in traditional HDS (HDN) processes that could be suitable also for HDO process.

The aim of this study is to investigate the effect of lithium in a Li-modified NiMo/Al_2O_3 catalyst prepared from the ammonium salt of Anderson compound $(NH_4)_4NiMo_6O_{24}H_6$ (abbreviated $NiMo_6$). We decided to investigate such catalysts in HDS of thiophene to reveal whether the effect of lithium on the Al_2O_3-supported NiMo catalyst would be similar to that of NiMo/SiO_2 catalysts. These catalysts showed higher activity in HDS of thiophene with increasing Li concentration [9], which was very likely due to the stabilization of molybdenum dispersion induced by lithium loaded on SiO_2 support.

It was previously found [30] that lithium in the Al_2O_3-MgO-supported CoMo catalysts can enhance the selectivity of direct desulfurization in HDS and promote not only the reduction of the number of acidic sites but also the reduction of the acid strength of these sites [31]. Therefore, we decided to study Li-modified NiMo/Al_2O_3 catalysts in the hydrotreating of a model reaction mixture, namely 1-benzothiophene and octanoic acid, representing a mixture of petroleum fractions and fatty feedstocks. This study would be of great interest since the different acid–base properties of the NiMo/Al_2O_3 catalysts due to Li modification could be observed in both reactions.

Therefore, in this paper, the formation of molybdenum phases, their physical properties and activities in the hydrorefining reactions of model feeds are investigated. The study shows how lithium content in the range of 0.1–1.3 wt.% affects the activity in HDS of thiophene at 300–370 °C and 1.0 MPa and the activity in parallel HDO/HDS of octanoic acid (OA) and 1-benzothiophene (BT) at 330 °C and 1.6 MPa.

2 Experimental

2.1 Preparation of Catalysts

Basically, catalyst support (grains γ- Al_2O_3 with diameter 0.16–0.32 mm, $S_{BET} = 184\ m^2g^{-1}$, $V_{tot} = 0.505\ cm^3g^{-1}$, Euro Support Manufacturing Czechia, s.r.o, Litvínov, Czech Republic) was impregnated with an aqueous solution of Anderson's salt $(NH_4)_4NiMo_6O_{24}H_6$) prepared according to Tsigdinos by reacting solutions of ammonium molybdate and nickel sulfate at 80 °C [32]. Prior to the deposition of the active components onto alumina, the support was impregnated with an aqueous $Ni(NO_3)_2$ solution, dried and calcined at 350 °C for 4 h to ensure sufficient Ni in the resulting catalysts (−1.5 wt.%). The support thus prepared was impregnated with an aqueous solution of Anderson's salt and Li_2CO_3 at a temperature of about 80 °C. (Preparation of 5 g of NiMo6-0.1 sample: 0.28 g of Anderson salt + 0.053 g of Li_2CO_3 was dissolved in 40 ml of water and then a pre-prepared Al_2O_3 carrier containing about 1.5 wt.% Ni was added to this solution. The suspension was evaporated with stirring at 60 °C and 70 Pa to dryness on a vacuum evaporator. The resulting product was dried at 105 °C for about 8 h and subsequently calcined at 350 °C for 4 h. All impregnated samples were dried 4 h at 105 °C and calcined in a crucible furnace at a heating rate of 6 °C min^{-1} and then at 350 °C for 4 h. After calcination, the prepared catalysts were designated as $NiMo_6$-x, where x indicates the amount of lithium (wt.%) in the calcined catalyst.

2.2 Characterization of the Catalysts

The content of metals in the prepared catalysts was determined by Agilent 4200 MP-AES (atomic emission spectroscopy with microwave plasma) after samples dissolution in diluted (2%) hydrochloric acid.

Nitrogen physisorption on catalyst (grain size 0.16–0.32 mm) was performed using an ASAP 2020 Micromeritics instrument after degassing at 350 °C and 1 Pa vacuum for 24 h. The adsorption–desorption isotherms of nitrogen at -196 °C were evaluated by the standard Brunauer–Emmett–Teller (BET) procedure [33] for the p/p_0 range = 0.05–0.25 to calculate the specific surface area S_{BET}. Total pore volume, V_{total}, was determined from nitrogen adsorption isotherm at p/p_0 (−0.995). The measurements of S_{BET} and V_{total} are made with an accuracy of ± 2%. The pore-size distribution (pore radius 10^0–10^2 nm) was evaluated

from the adsorption branch of the nitrogen isotherm by the Barrett–Joyner–Halenda (BJH) method [34] assuming a cylindrical pore geometry. The Lecloux–Pirard standard isotherm [35] was used for the *t*–plot and for the pore–size distribution evaluation. Volume of micropores, V_{micro}, and pore radius, *R*, were determined.

Temperature-programmed reduction (H_2-TPR) measurements were performed with the H_2/N_2 mixture (10 mol.% H_2), flow rate of 50 ml min^{-1}, and a linear temperature increase of 20 °C min^{-1} up to 800 °C. Changes in H_2 concentration were detected with a catharometer. Reduction of grained CuO (0.16–0.32 mm) was performed to calculate absolute values of the hydrogen consumed during reduction of the samples [6].

Temperature-programmed NH_3 desorption (NH_3–TPD) was performed to investigate the acidic properties of the catalyst surface [6, 36, 37], as it has been previously shown that Broensted sites are not present in Al_2O_3-supported NiMo catalysts [38]. Thus, the adsorption of pyridine on lithium-modified NiMo/Al_2O_3 catalysts has not been investigated. The NH_3-TPD measurements were performed with a 0.5 g sample in the temperature range of 20–650 °C, with helium (16 ml min^{-1}) as a carrier gas and NH_3 as the adsorbing gas. Prior to the NH_3-TPD measurement, the sample was heated in helium from 25 to 500 °C, with a temperature ramp of 20 °C min^{-1}; then, the sample was cooled in helium to 25 °C. Ten doses of NH_3, 840 µl each, were applied to the catalyst sample at 30 °C before flushing with helium for 1 h and heating at the rate of 20 °C min^{-1}. The composition of gases evolved during the experiments was determined by a mass spectrometer (Balzers). The mass contributions *m/z 16*–NH_3 was collected. The spectrometer was calibrated by dosing the known amount of NH_3 into the carrier gas (He) in every experiment. Identical apparatus and experimental conditions were used for the measurements of catalyst basicity (CO_2-TPD), only CO_2 was used instead of NH_3. The mass contributions *m/z 44*–CO_2 was collected. The H_2-TPR, NH_3-TPD, and CO_2-TPD experiments were evaluated using OriginPro 8.0 software with the accuracy of ± 5%.

An Avatar 360 (Nicolet) FTIR spectrometer was used to obtain infrared spectra from catalysts between 360 and 4000 cm^{-1} (resolution 1.93 cm^{-1}, 300 scans, 1 s per scan, transmission mode) when the sample powder was pressed with KBr into a pellet. The spectrum of the support was eliminated using a compensation method [39].

The XPS measurements were performed in the analysis chamber of the electron spectrometer ESCALAB-Mk II (VG Scientific) with a base pressure of ~ 5×10^{-8} Pa. The "as–prepared" calcined samples in powder form were pressed into graphite covered copper sample holders, the pellets so obtained had diameter of 10 mm and thickness −1.5 mm. The C 1 s, O 1 s, Al 2p, Li 1 s, Mo 3d, and Ni 2p photoelectron lines were recorded with AlK_α ($h\nu = 1486.6$ eV) radiation. All spectra were calibrated using O 1 s peak at 531.5 eV as a reference. The surface composition was evaluated from the photoelectron intensities divided by the corresponding photoionization cross sections taken from Scofield [40]. In order to check at least qualitatively the uniformity of active phase distribution in the bulk of the alumina support, additional measurements of samples crushed in agate mortar before analysis were also performed.

The model reaction was gas-phase hydrodesulfurization of thiophene (Th) in a fixed-bed flow reactor at the total pressure of 1.0 MPa. The feed rate of Th, F_{Th}, was 0.909 mmol h^{-1}, and that of hydrogen, F_{H2}, was 0.732 mol h^{-1}. The catalyst charge, *W*, was 0.01 g. The catalyst was pre–sulfided in situ by a mixture of H_2S/H_2 (1:10) at atmospheric pressure with a flow rate of 110 ml min^{-1}, a temperature rise rate of 6 °C min^{-1} to 400 °C and dwell time of 1 h. These pre-sulfidation conditions represent typical conditions for the formation of sulfide catalysts from oxide precursors. The sulfidation process is documented in [41] and references therein. The Th conversion, x_{Th}, was determined at 300, 340, and 370 °C. The conversion was defined as $x_{TH} = (n^o_{Th} - n_{Th})/n^o_{Th}$, where n^o_{Th} and n_{Th} are the initial and final number of moles of Th, respectively. The activity of catalyst was evaluated as a pseudo-first-order rate constant k_{Th} ($mmol_{Th}\ g_{cat}^{-1}\ h^{-1}$) of Th conversion:

$$k_{Th} = -\left(F_{Th}/W\right) \ln\left(1 - x_{Th}\right) \quad (1)$$

Parallel deoxygenation and desulfurization was carried out on a fixed-bed flow reactor at 330 °C and 1.6 MPa using the previously reported method [27]. Briefly, catalysts were pre–sulfided in situ as it was described above. The feed consisted of octanoic acid (OA), 1-benzothiophene (BT), decane and H_2. The composition of the feed was kept constant at 16, 16, 200, and 1368 kPa of OA, BT, decane, and H_2, respectively. The catalyst weight (*W*) was 0.06 and 0.1 g. The reaction was performed at three feed rates of OA and BT (F_{OA} and F_{BT}): 7.7, 10.3, and 15.5 mmol h^{-1}. The conversion of OA was defined as $x_{OA} = (n^o_{OA} - n_{OA})/n^o_{OA}$, where n^o_{OA} and n_{OA} are the initial and final number of moles of OA, respectively. Yields y_{C7+C8} were defined as $y_{C7+C8} = (n_{C7} + n_{C8})/n^\circ_{OA}$, where n°_{OA} and *n* are the initial moles of octanoic acid and the moles of the linear hydrocarbons, respectively. The total hydrodeoxygenation (HDO) activity was quantified as empiric pseudo-first order rate constant k_{HDO} of the sum of the yields of linear C_7 and C_8 hydrocarbon formation y_{C7+C8}. The total HDO activity k_{HDO} ($mmol_{(C7+C8)}\ g_{(cat)}^{-1}\ h^{-1}$) was achieved by non–linear fitting from the dependence of y_{C7+C8} on W/F_{OA}:

$$y_{C7+C8} = 1 - \exp\left(-k_{HDO} * W/F_{OA}\right) \quad (2)$$

The hydrodesulfurization (HDS) activity during HDO/HDS was quantified as the empiric pseudo-first order rate

constant of the k_{HDS} yields of ethylbenzene (EB) formation y_{EB}. The BT conversion was defined as $x_{BT}=(n^{o}_{BT}-n_{BT})/n^{o}_{BT}$, where n^{o}_{BT} and n_{BT} are the initial and final moles of BT, respectively. The yield y_{EB} was defined as $y_{EB}=(n_{EB})/n^{\circ}_{BT}$, where n°_{BT} and n_{EB} are the initial amount of 1-benzothiophene and the amount of ethylbenzene, respectively. The HDS activity k_{HDS} ($mmol_{EB}\ g_{(cat)}^{-1}\ h^{-1}$) was obtained by a non-linear fitting from the dependence of y_{EB} on W/F_{BT}:

$$y_{EB} = 1-\exp\left(-\mathrm{k_{HDS}} * W/F_{BT}\right) \quad (3)$$

3 Results

3.1 Physical–Chemical Properties of the Prepared Catalysts

The chemical composition of $NiMo_6$-x catalysts (calcined at 350 °C for 4 h) prepared from the ammonium salt of polyoxonickelate and a small amount of Li_2CO_3 is shown in Table 1. The concentration of lithium was gradually increased from 0 wt.% for the $NiMo_6$-0 sample to 1.3 wt.% for the $NiMo_6$-1.3 sample. The concentration of Ni was around 1.5 wt.%. The concentration of molybdenum was around 8.5 wt.%. The molar ratio of Ni/Mo in the catalysts was close to 0.28.

The porous structure of the Li-doped $NiMo_6$ catalysts was characterized by adsorption/desorption of nitrogen at –196 °C and the results are summarized in Table 2. The S_{BET} surface area of all catalysts was lower than the surface area of the support (184 $m^2\ g^{-1}$, $V_{tot}=505\ mm^3_{liq}\ g^{-1}$), which was due the partial blocking of small pores during the impregnation of the support with active components. The surface area of the catalyst without lithium showed the value approximately 167 $m^2\ g^{-1}$. This value therefore represents a surface area of about 192 $m^2\ g^{-1}$ after normalization per gram of support.

However, the addition of a small amount of lithium decreased the surface area of the catalysts slightly; the catalyst with 0.9 wt.% Li showed the smallest surface area ($S_{BET}=153\ m^2\ g^{-1}$). Accordingly, the total pore volume decreased with increasing Li concentration in the solids from 425 to 396 $mm^3_{liq}\ g^{-1}$. The V_{micro} micropore volume was small in all cases (about 2% of the total pore volume). Experimental data show that increasing lithium concentration higher than 1.0 wt.% in the catalysts have a negative effect on the porous structure of metal oxides.

Table 2 Characteristic values of porous structure of the examined samples

Sample	S_{BET} $m^2\ g^{-1}$	V_{total} $mm^3_{liq}\ g^{-1}$	V_{micro} $mm^3_{liq}\ g^{-1}$	R nm
$NiMo_6$-0	167	424	8	5.0
$NiMo_6$-0.1	158	411	6	5.0
$NiMo_6$-0.2	156	438	7	5.4
$NiMo_6$-0.9	153	396	7	5.2
$NiMo_6$-1.3	174	425	6	4.7

S_{BET} Surface area determined from N_2 adsorption isotherm at $T=-196$ °C; V_{total} Total pore volume determined from N_2 adsorption isotherm at $P/P_0=0.995$; V_{micro} Volume of micropores determined by *t*-plot method using standard isotherm of Lecloux and Pirard; *R* Pore radius determined from a maximum at pore-size distribution curve

The nitrogen adsorption–desorption isotherms obtained with calcined catalysts confirm that there is not a significant difference in the pore size distribution among the catalysts with lithium concentrations ranging from 0.1 to 1.3 wt.% (see Fig. S.1 in Supplementary Information). Very similar pore radii (around 5 nm) were observed for the $NiMo_6$-0 and $NiMo_6$-0.1 catalysts, while the other two catalysts ($NiMo_6$-0.2, $NiMo_6$-0.9) showed slightly larger pore radii (5.4 and 5.2 nm). The data show that the content of lithium in catalysts higher than about 1 wt.% leads to a decrease in pore radius due to sintering. The pore characteristics changed only slightly for the sample with 1.3 wt.% Li, probably due to the interaction of Li^+ with isolated MoO_4^{2-} ions leading to the formation of new poorly dispersed Li_2MoO_4 crystallites [42].

Reduction of the prepared $NiMo_6$-x catalysts containing various amount of lithium was studied by H_2-TPR in the temperature range of 25–800 °C (Fig. 1). The reduction of unsupported Anderson salt was carried out in three regions with temperature maxima at 492, 620 and > 800 °C.

Table 1 Chemical composition, H_2 consumption during H_2–TPR, and amounts of NH_3 and CO_2 desorbed during NH_3–TPD and CO_2–TPD experiments

Sample	Li wt.%	Ni wt.%	Mo wt.%	Ni/Mo mol mol^{-1}	H_2–TPR[a] mmol g^{-1}	NH_3–TPD[a] mmol g^{-1}	CO_2–TPD[a] mmol g^{-1}
$NiMo_6$-0	0	1.49	8.61	0.28	0.62	0.60	0.01
$NiMo_6$-0.1	0.09	1.50	8.70	0.28	0.59	0.64	0.01
$NiMo_6$-0.2	0.18	1.48	8.61	0.28	0.52	0.53	0.01
$NiMo_6$-0.9	0.89	1.65	9.85	0.27	0.29	0.29	0.04
$NiMo_6$-1.3	1.32	1.37	6.95	0.32	0.23	0.21	0.09

[a]Upto 500 °C

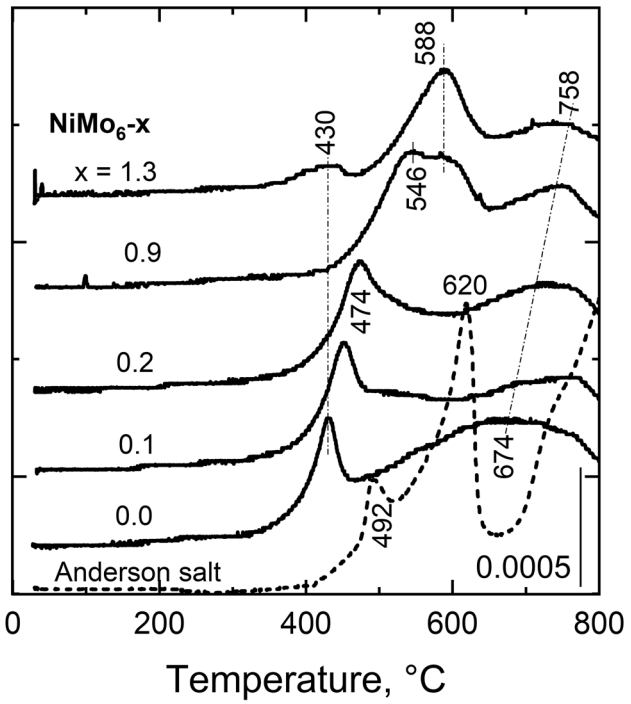

Fig. 1 H2–TPR profiles of unsupported Anderson salt and NiMo6-x catalysts with different amounts of Li (x is given in wt.%)

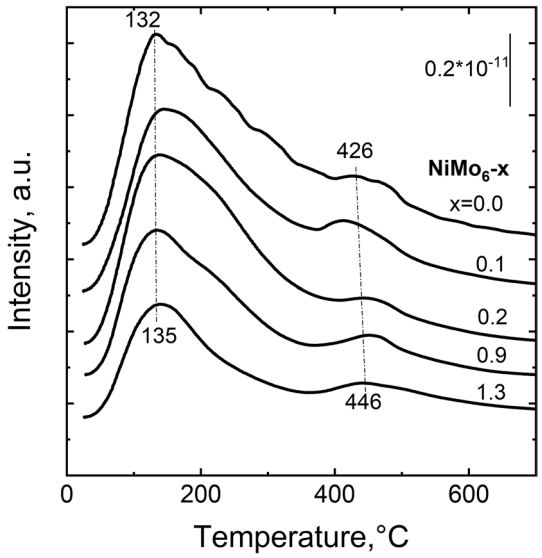

Fig. 2 NH_3–TPD profiles of NiMo6-x catalysts modified with different amounts of lithium (x = Li content in wt.%)

According to Cabello et al. [43] who investigated the reduction process of $(NH_4)_3CoMo_6H_6O_{24}.7\ H_2O$ Anderson phase, two main reduction regions representing the $Mo^{VI} \rightarrow Mo^{IV}$ and $Mo^{IV} \rightarrow Mo^0$ reactions were found. Thus, in our case, the peak at 620 °C represents the reduction of $NiMoO_4$ to MoO_2 and the peak at temperature higher than 800 °C represents the reduction of MoO_2 to Mo. The small peak observed at 492 °C can be attributed to the reduction of Mo_4O_{11}, which is formed as an intermediate in the reduction process. After deposition of Anderson salt on Ni/γ–alumina support, all catalysts exhibit two typical temperature regions of H_2 consumption with increasing temperature. For $NiMo_6$-x catalysts, we can observe significant changes in the temperature peaks with increasing Li concentration. The lithium-free catalyst ($NiMo_6$-0) showed temperature peaks at 430 and 674 °C, roughly separated at about 450 °C. Higher Li content led to a shift of the low temperature peak to higher temperatures and to its broadening. The catalyst with the highest Li concentration ($NiMo_6$-1.3) showed three reduction peaks with maxima at 430, 588, and 758 °C. Thus, the T_{max} positions of the reduction peaks in H_2–TPR (Table 1) reflected the Li concentration in the $NiMo_6$-x catalysts: increasing Li concentration led to delayed reduction of metal oxides. The intensity of the reduction peaks decreased with increasing Li concentration. At the same time, the value of the peak position increased. The progression of the reduction peaks indicates a gradual change in the composition of the catalysts due to the addition of Li, and the formation of compounds such as $NiMoO_4$ and MoO_2 and compounds formed during interaction of POM with the support.

The acidity of the catalysts is an important factor that affects the chemical reactivity of the reactants due to the different acidic nature of the catalyst surface and the reacting molecules. Several types of acid sites can be recognized in the NH_3-TPD profiles of oxide catalysts. Weakly acidic sites are attributed to –OH groups occurring on the catalyst surface, moderately acidic sites are formed by metal(Me)-bound oxygen as Me^{2+}–O^{2-} or Me^{3+}–O^{2-} pairs, and strongly acidic sites are attributed to isolated cations [44]. Individual peaks below 140 °C can be assigned to weakly acidic sites, peaks appearing in the range 140–220 °C to moderately acidic sites, and peaks above 270 °C can be assigned to strongly acidic sites. Protons present in 6-heteropoly anions such as $[NiMo_6O_{24}H_6]^{4-}$ are directly bound to oxygen atoms bridging Ni and Mo atoms and are not neutralized prior to the decomposition of these anions by the base.

NH_3-TPD measurements were performed to determine the differences in acidity between fresh $NiMo_6$-x catalysts modified by lithium and calcined at 350 °C. The effect of lithium content on the amount of acid sites is shown in Table 1 and Fig. 2. The NH_3-TPD desorption profiles represent all types of acid sites – weak, medium, and strong—but

a strict separation between them was not possible. In the lithium-free catalyst ($NiMo_6$-0), weak and moderately acidic sites were predominant. The $NiMo_6$-0.1 catalyst with the lowest Li concentration (0.09 wt.%) showed a very similar NH_3 desorption profile to the $NiMo_6$-0 catalyst.

A significant increase in Li concentration (0.9 wt.%) led to a gradual decrease in the amount of weakly acidic sites with a maximum desorption at 132 °C (Fig. 2), but the strongly acidic sites corresponding to NH_3 desorption at ca. 426 °C were still retained in the catalyst. An even higher concentration of lithium in the catalyst (1.3 wt.%) led to a significant reduction in the amount of weakly and strongly acidic sites desorbing at 132 and 426 °C. Thus, the NH_3 desorption of the $NiMo_6$-1.3 catalyst differed substantially from the other catalysts (Fig. 2), as it showed the lowest amount of very strong acid sites characterized by a T_{max} of NH_3 desorption around 470 °C.

Desorption of CO_2 at increasing temperature was chosen as a method to characterize the basicity of the catalysts (Fig. S2). The course of CO_2 desorption from catalysts with low Li concentration is practically the same as for the unmodified catalyst. The addition of 0.09 wt.% Li caused a shift of CO_2 desorption to lower temperatures, indicating a shift of the strength of the basic sites to lower values. A more pronounced shift of desorption to lower temperatures can be seen in case of the catalyst with 1.3 wt.% Li. The temperature maximum has shifted from 550 to 450 °C. In addition, this catalyst showed a significant presence of weak base sites (temperature maximum of CO_2 desorption at about 100 °C). The basicity (Table 1) expressed as mmol CO_2 g^{-1} desorbed from 25 to 500 °C showed very low values, ranging from 0.01 for the unmodified catalyst to 0.09 mmol g^{-1} for the catalyst with 1.3 wt.% Li. These data demonstrate the amphoteric nature of POM- prepared catalysts, which shifted to basic nature after the introduction of ≥ 0.9 wt.% Li.

Fourier transform infrared spectroscopy (FTIR) identifies different types of molecular bonds present in solid samples. In our catalysts, stretching mode bands in the range 3200–3600 cm^{-1} and 1600–1750 cm^{-1} (not shown here) appeared due to the presence of crystallization and constitution water, with higher amounts in $NiMo_6$-0.9 and $NiMo_6$-1.3 catalysts than in $NiMo_6$-0, $NiMo_6$-0.1 and $NiMo_6$-0.2 catalysts. Figure. 3 shows the FTIR spectra of the calcined catalysts taken in the region from 400 to 1200 cm^{-1}.

Two broad bands at about 900 cm^{-1} (with close bands at 875 and 926 cm^{-1}) and 636 cm^{-1} (with a shoulder at 575 cm^{-1}) are characteristic of the synthesized Anderson polyoxomolybdate (POM) and correspond well with the bands described in the literature [45, 46]. The absorption

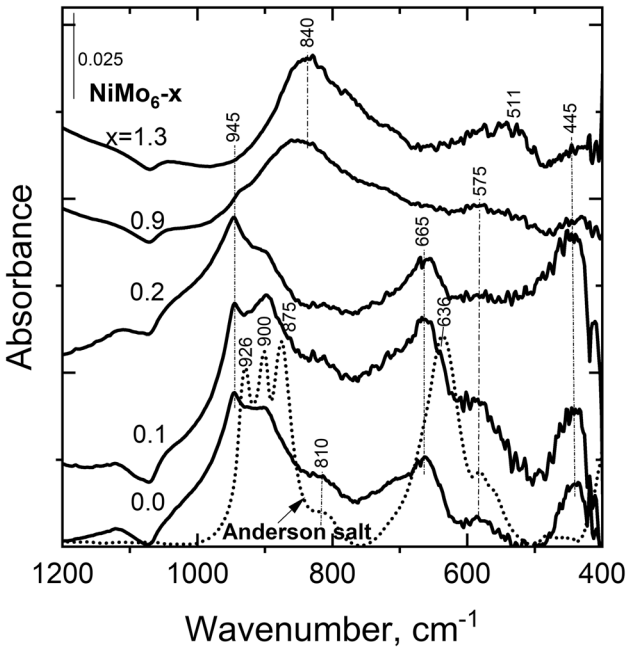

Fig. 3 FTIR spectra of Anderson salt and $NiMo_6$–x catalysts modified with lithium (x = Li content in wt.%); the spectrum of the support is subtracted

bands at ca. 950–850 cm^{-1} are attributed to cis–MoO_2 bonds and the bands at 636–500 cm^{-1} are attributed to bridging Mo–O–Mo bonds.

After deposition of nickel polyoxomolybdate $(NH_4)_4NiMo_6O_{24}H_6$ on Ni/Al_2O_3, the bands of $NiMo_6$-0 catalyst were slightly shifted to higher wavenumbers (665, 900 and 945 cm^{-1}), and a new band at 445 cm^{-1} appeared. These bands are in agreement with the bands found for $(NH_4)_3AlMo_6O_{24}H_6$ [39], which may have formed during the catalyst preparation due to the interaction between the Ni/Al_2O_3 and the active component $(NH_4)_4NiMo_6O_{24}H_6$. These species could also be formed by interaction of Ni and Mo compounds with partially dissolved alumina domains during impregnation [47, 48].

Very similar spectra were observed for the $NiMo_6$-0.1 and $NiMo_6$-0.2 catalysts with Li concentration < 0.2 wt.%; only the band at 945 cm^{-1} is more pronounced for the $NiMo_6$-0.2 catalyst.

The increasing Li concentration in the catalysts (0.9 and 1.3 wt.%) was reflected by the disappearance of the characteristic Anderson salt bands and the appearance of new broad bands at 840 cm^{-1} (attributed to lithium molybdate formation) and a not very strong band at 511 cm^{-1}. It is evident that the original Anderson salt was broken during the preparation of catalyst and new compounds

may have formed on the support surface. Based on the position of the determined bands, NiO and/or Li_2O could have been present in the catalysts after calcination, since the bands appearing below 600 cm^{-1} can be attributed to metal–oxygen–metal (M–O–M, where M = Ni or Li) bonding [49]. Bielanski et al. [50] reported on the basis of their FTIR measurements that no Lewis-acid sites are present in the ammonium salts of Keggin type heteropoly-acid $H_3P_{12}MoO_{40}$, even after processing at 400 °C. Thus, only Brönsted acidity is present, which is due to protons originating from hydrogen bonds between the Keggin units and not to typical OH groups such as those in acid zeolites or alumina. A similar situation in acidity can be expected for the Anderson salt.

The chemical state and composition of the oxidized and freshly sulfided (400 °C) catalysts were investigated by XPS technique. The binding energies of the elements in the calcined samples are given in Table 3. Values in brackets refer to samples that were crushed in an agate mortar prior to analysis. The values found for Mo $3d_{5/2}$ (233 eV) and Ni $2p_{3/2}$ (856.6 eV – main line) are typical for oxidation state of Mo^{6+} and Ni^{2+} (in the oxide matrix). The surface concentrations of all elements in the calcined as-prepared and crushed samples are given in Table 4.

The surface concentration of Ni and Mo after crushing the samples shows only a small decrease (about 10 – 12%) compared to the concentration in the as-prepared samples. This indicates a uniform distribution of the active phase in the catalyst support grains. It is clear that the surface is enriched in both Ni and Mo, when comparing these quantities with the bulk analysis. Due to the low photoelectric cross section for lithium [40] peak feature was observed only for the $NiMo_6$-0.9 and $NiMo_6$-1.3 samples, whose binding energy corresponds to the Li_2CO_3 compound [51]. The correctness of the assignment is demonstrated by the higher intensity at 289.5 eV in the C 1 s region for these two samples, which also indicates the presence of carbonate species on the surface. Another explanation for the Li peak could be the presence of $LiNiO_2$ on the surface. However, the Ni $2p_{3/2}$ binding energy (main line) for $LiNiO_2$ (i.e., Ni^{3+}) shows a value about 1 eV lower [51] compared to Ni^{2+}. Therefore, the very small shift (0.1 eV) observed for the $NiMo_6$-0.9 and $NiMo_6$-1.3 samples (see Table 3) in this direction cannot be considered as evidence for the presence of a $LiNiO_2$–like species on the surface.

Mo 3d spectra for the calcined samples are shown in Fig. 4. It is worth mentioning the high sensitivity of all samples to X–rays in vacuum. After a few minutes of irradiation, the samples darken, and therefore lower power (30 W instead of 230 W) was used during data acquisition to reduce the observed effect. Peak features at ~ 232 eV indicate partial reduction of molybdenum during analysis. Samples with higher lithium content were more stable and remained virtually unchanged during analysis. To test this idea, we performed an additional study of the effect of X–ray irradiation for the sample $NiMo_6$-0.1. After prolonged irradiation under vacuum at high power, the surface portion of the sample was scraped off and analyzed by ESR spectroscopy. The

Table 3 Binding energies of elements in oxide catalysts (eV)

Sample	$NiMo_6$-0	$NiMo_6$-0.1	$NiMo_6$-0.2	$NiMo_6$-0.9	$NiMo_6$-1.3
Al 2p	74.8 (74.7)	74.8 (74.7)	74.8 (74.7)	74.7 (74.7)	74.7 (74.6)
Mo $3d_{5/2}$	233.2 (233.1)	233.0 (233.0)	233.1 (233.2)	232.9 (232.9)	232.9 (232.9)
Ni $2p_{3/2}$ (main line)	856.7 (856.7)	856.7 (856.7)	856.6 (856.7)	856.4 (856.6)	856.4 (856.5)
O 1 s	531.5 (531.5)	531.5 (531.5)	531.5 (531.5)	531.5 (531.5)	531.5 (531.5)
Li 1 s				55.2 (55.2)	55.4 (55.4)

The values in parentheses are for samples crushed in an agate mortar before analysis

Table 4 Surface composition of oxide catalysts (at. %) determined by X–ray photoelectron spectroscopy and the ratio of surface (XPS) and bulk analysis (chemical analysis) for Ni and Mo

Name	$NiMo_6$-0	$NiMo_6$-0.1	$NiMo_6$-0.2	$NiMo_6$-0.9	$NiMo_6$-1.3
Ni 2p	0.96 (0.95)	1.01 (0.8)	0.94 (0.87)	0.85 (0.83)	0.73 (0.58)
Mo 3d	2.97 (2.65)	2.99 (2.76)	3.19 (2.76)	2.69 (2.46)	1.8 (1.61)
Al 2p	37.11 (37.05)	36.4 (37.51)	36.81 (37.57)	34.19 (34.68)	34.84 (35.12)
O 1 s	58.96 (59.35)	59.59 (58.93)	59.07 (58.79)	57.48 (58.86)	59.42 (57.45)
Li 1 s				4.78 (3.17)	3.2 (5.24)
Mo/Al	0.08 (0.08)	0.082 (0.074)	0.087 (0.073)	0.079 (0.071)	0.052 (0.046)
Ni/Mo	0.32 (0.36)	0.34 (0.29)	0.29 (0.31)	0.32 (0.34)	0.4 (0.36)
Ni: Surface/bulk, wt.%/wt.%	1.66	1.75	1.61	1.39	1.48
Mo: Surface/bulk, wt.%/wt.%	1.44	1.45	1.54	1.2	1.17

The values in parentheses are for samples crushed in an agate mortar before analysis

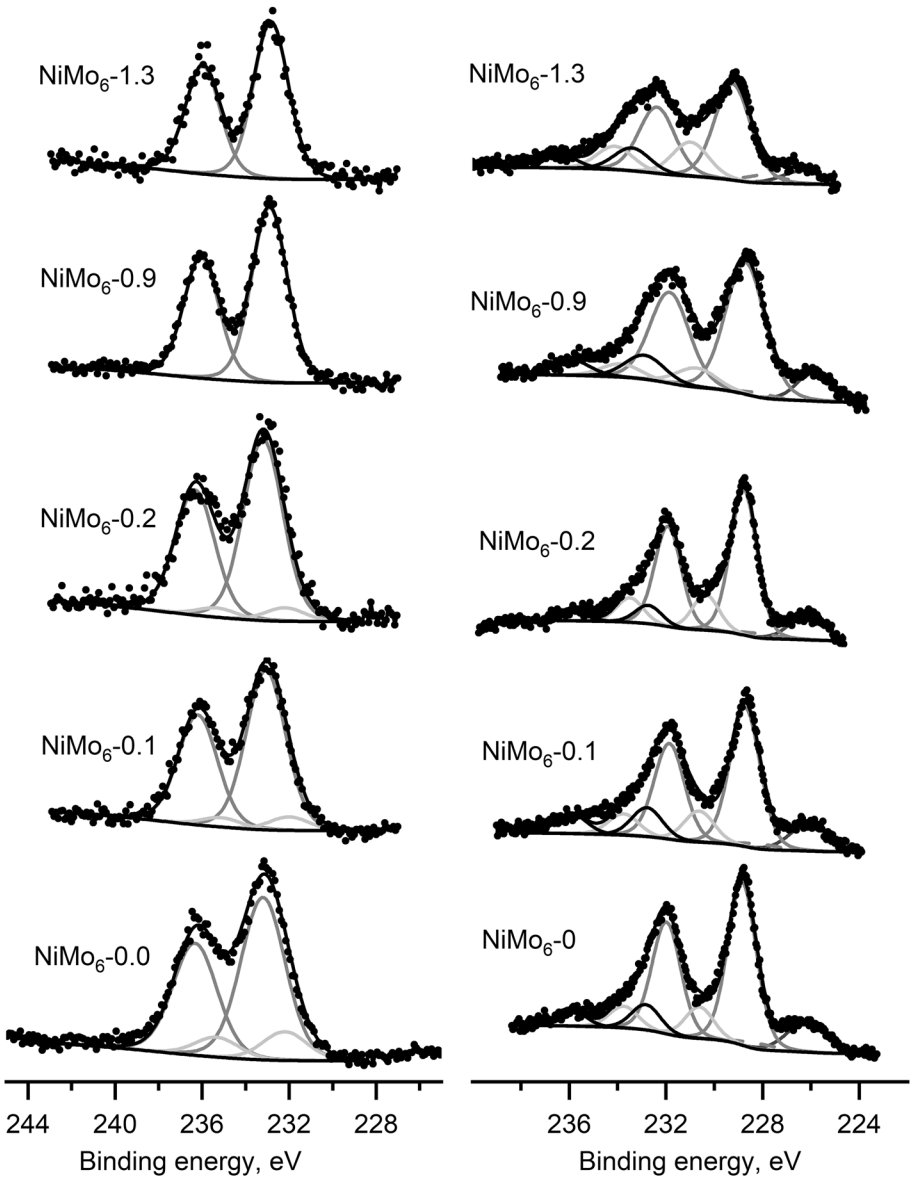

Fig. 4 Peak fitting of Mo 3d spectra for the as-prepared samples in oxide (left) and sulfidic (right) form. In order to minimize the effect of X-ray irradiation during data acquisition, the X–ray source was set to a lower power (5 mA/6 kV = 30 W)

ESR result (not shown here) clearly showed the presence of Mo^{5+}, which was not observed in the "fresh" sample. Based on this observation, it can be concluded that the components showing lower binding energy in the Mo 3d spectra are due to X–ray irradiation during XPS analysis.

After sulfidation of the samples, the Mo3d XPS line has a complex structure. For Mo $3d_{5/2}$, it is represented by three fitting peaks (Fig. 5, right) with binding energies of 228.7–229.2 eV, 230.4–231.0 eV and 232.7–233.4 eV (Table 5), which correspond to Mo^{4+} ions in MoS_2, Mo^{5+} ions in Mo oxysulfide forms such as MoO_xS_y, and Mo^{6+} ions (as in MoO_3), respectively. These Mo $3d_{5/2}$ peaks were accompanied by Mo $3d_{3/2}$ peaks at about 3 eV higher binding energy.

Spectra decomposition of Ni 2p line showed two peaks; at 853.8 eV assigned to Ni^{2+} ions in NiS_x and at 856.7 eV indicating the presence of Ni^{2+} ions as in oxidic samples (Table 5), but the data are burdened with a large error due to the low Ni concentration. The S 2p line was fitted with two S 2p fitting peaks: the first peak with binding energy S $2p_{3/2}$ 161.1–161.8 eV corresponds to S^{2-} ions in the MoS_2 and/or NiS phase, the second at 162.2–162.8 eV to S_2^{2-} ions in the Mo oxysulfide form (Fig. 5). Note the shift of the S $2p_{3/2}$ peak in the sulfided $NiMo_6$-0.9 and $NiMo_6$-1.3 samples by 0.5–0.6 eV to lower binding energy values compared to the same S $2p_{3/2}$ peak in the other samples. Some authors attribute a similar shift to the formation of the K-intercalated MoS_2 phase in the supported

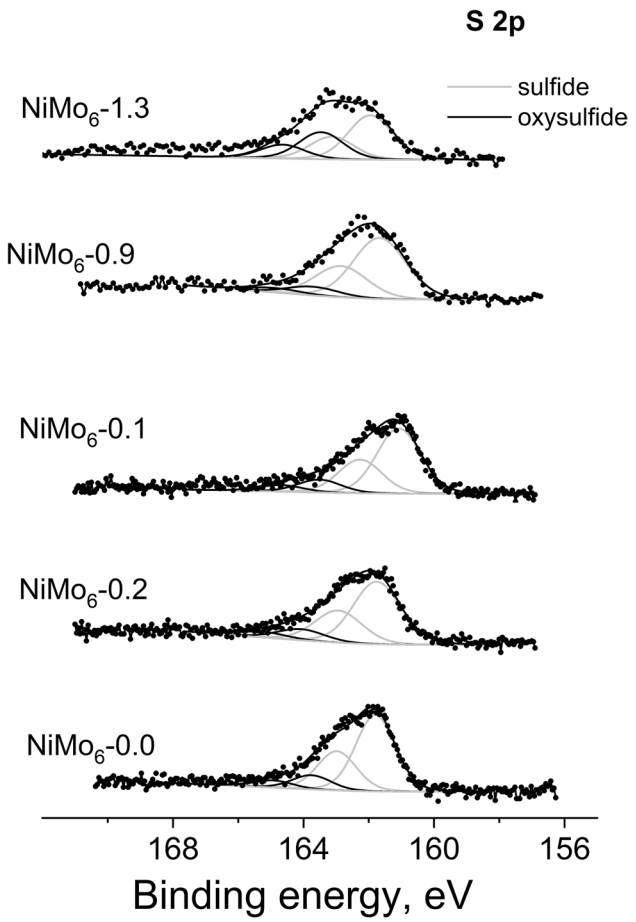

Fig. 5 Peak fitting of S 2p spectra of the sulfided catalysts

K-Mo samples [52]. However, we did not observe a parallel shift to the lower BE of Mo $3d_{5/2}$ line. We assume that Li can modify the electronic properties of the MoS_2 phase in Li-$NiMo_6$ samples and can form Li_xMoS_2 in close interaction with it.

Regarding the surface atomic concentrations of the elements, the presence of Li in the catalysts caused a decrease in the degree of sulfidation of Mo and Ni (Table 6). This may be due to the formation of tetrahedral forms of Mo species [30] that interact strongly with the support, as seen in the TPR profiles (Fig. 1). The sample with the highest Li content showed the lowest degree of sulfidation of Mo (62.8%) estimated from the Mo^{4+}/M_{tot} ratio (Table 6). The degree of sulfidation of Mo for the other samples ranged from 70 to 75%. After sulfidation, Mo was stabilized on the surface of catalysts with higher Li content (0.9–1.3 wt.%), as Mo/Al ratio did not decrease. On the other hand, Ni dispersion increased after sulfidation for all samples (Table 6, Ni/Al ratio). The observed S/Mo ratio was higher than 2 for all samples.

As for NiS_x species, their proportion (Table 6) was 81.8% for the $NiMo_6$-0.1 sample and 75.0% for the other Li-containing samples. Thus, in the samples with higher Li content (0.2–1.3 wt.%), 25% of NiO_x species remained unsulfided, while in the NiMo6-0.1 sample, its proportion was only 18.2%. The proportion of S^{2-} ions present in the MoS_2/NiS_x phases of the samples was 83–87%, except for the $NiMo_6$-1.3 sample where 62% was recorded.

The proportion of unsulfided MoO_3 in the NiMo6-0.1 sample was only 9.2%, which is the lowest value among all samples. The proportion of partially sulfided MoO_3, MoO_xS_y, was 18% in the $NiMo_6$-0.1 sample, which was higher than that of the $NiMo_6$-0.2 and $NiMo_6$-0.9 samples. Since the proportion of MoS_2 active phase in $NiMo_6$-0.1 was approximately 73%, the sum of the sulfide MoO_xS_y and MoS_2 components was 90.8%, which was the highest value found among all the samples.

3.2 Activity of the Catalysts

3.2.1 HDS of Thiophene

The effect of lithium on the catalytic activity of supported NiMo catalysts in the hydrodesulfurization of thiophene was studied on the catalysts prepared from Ni Anderson salt

Table 5 Binding energies (eV) and (in parentheses) surface atomic concentration (at. %) of elements in sulfided catalysts

Sample	$Mo3d_{5/2}$ Mo^{4+}	$Mo3d_{5/2}$ Mo^{5+}	$Mo3d_{5/2}$ Mo^{6+}	$S2p_{3/2}$ S^{2-}	$S2p_{3/2}$ S_2^{2-}	$Ni2p_{3/2}$ NiS_x	$Ni2p_{3/2}$ Ni oxide
$NiMo_6$-0.0	228.8 (22.6)	230.6 (4.4)	232.8 (3.5)	161.7 (58.7)	162.7 (10.9)	853.8 (0.9)	856.5 (0.2)
$NiMo_6$-0.1	228.8 (20.3)	230.4 (5.0)	232.7 (2.6)	161.6 (60.3)	162.8 (12.0)	853.7 (0.9)	856.7 (0.2)
$NiMo_6$-0.2	228.7 (21.0)	230.6 (4.7)	232.8 (4.4)	161.7 (59.5)	162.8 (10.6)	853.8 (0.9)	856.5 (0.3)
$NiMo_6$-0.9	228.7 (23.9)	230.7 (3.5)	232.9 (4.3)	161.2 (59.7)	162.2 (8.6)	853.8 (0.6)	856.7 (0.2)
$NiMo_6$-1.3	229.2 (18.9)	231.0 (6.7)	233.4 (4.5)	161.1 (43.5)	162.6 (26.5)	853.8 (0.6)	856.7 (0.2)

Table 6 Surface atomic ratio of elements in sulfided catalysts

Sample	$NiMo_6$-0.0	$NiMo_6$-0.1	$NiMo_6$-0.2	$NiMo_6$-0.9	$NiMo_6$-1.3
Ni/Al	0.034 (0.027)	0.032 (0.023)	0.039 (0.021)	0.031 (0.024)	0.029 (0.116)
Mo/Al	0.059	0.056	0.065	0.071	0.050
Ni/Mo	0.585	0.578	0.498	0.444	0.572
S/Mo	2.28	2.59	2.34	2.15	2.32
Mo^{4+}/Mo_{tot} %	66	60	68	70	62
MoS_2, %	74.0	72.8	69.8	75.4	62.8
MoO_xS_y, %	14.5	18.0	15.6	11.0	22.3
MoO_3, %	11.5	9.2	14.6	13.6	14.9
S^{2-}, %	84.3	83.4	84.9	87.4	62.1
S_2^{2-}, %	15.7	16.6	15.1	12.6	37.9
NiS_x, %	81.8	81.8	75.0	75.0	75.0

The Ni/Al ratio in the oxide form of the catalysts is given in parentheses

containing also different amounts of lithium. The reaction proceeds as follows:

$$\text{Thiophene} + 2H_2 = H_2S + \text{butane} \quad (4)$$

Butenes were not found in the reaction mixtures. The steady state thiophene conversions obtained with the $NiMo_6$-x catalysts containing different Li concentrations (x from 0 to 1.3 wt.%) at 300, 340, and 370 °C are summarized in Fig. 6. The thiophene conversion was highest for the Li-free catalyst, reaching 36.6, 67.5 and 84.5% at 300, 340 and 370 °C, respectively. However, the thiophene conversion decreased with increasing lithium concentration in the catalysts.

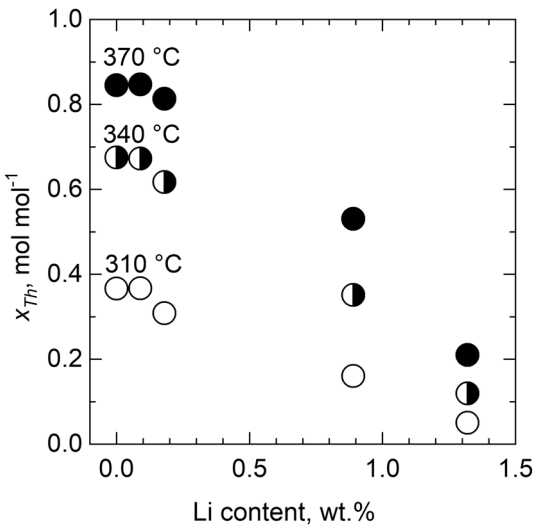

Fig. 6 Dependence of thiophene x_{TH} conversion in HDS reaction on the amount of lithium in NiMo6-x catalysts (x denotes Li content in wt.%) at three temperatures

3.2.2 Parallel HDO/HDS of Octanoic Acid and 1-Benzothiophene

Parallel deoxygenation and desulfurization was performed using octanoic acid (OA) and 1–benzothiophene (BT) as model reactants. During HDO/HDS, the following reactions took place:

$$1-\text{benzothiophene} + 2H_2 = H_2S + \text{ethylbenzene} \quad \text{hydrodesulfurization} \quad (5)$$

$$CH_3(CH_2)_6COOH = \text{n} - \text{heptane} + CO_2 \quad \text{decarboxylation} \quad (6)$$

$$CH_3(CH_2)_6COOH = \text{heptenes} + CO + H_2O \quad \text{dehydration}-\text{decarbonylation} \quad (7)$$

$$\text{heptenes} + H_2 = \text{n} - \text{heptane} \quad \text{hydrogenation} \quad (8)$$

$$CH_3(CH_2)_6COOH + 2H_2 = \text{octenes} + 2H_2O \quad \text{direct hydrodeoxygenation} \quad (9)$$

$$\text{octenes} + H_2 = \text{n} - \text{octane} \quad \text{hydrogenation} \quad (10)$$

The scheme of the reactions carrying out during HDS of thiophene and hydrodeoxygenation (HDO) of octanoic acid parallel with HDS of 1–benzothiophene is following:

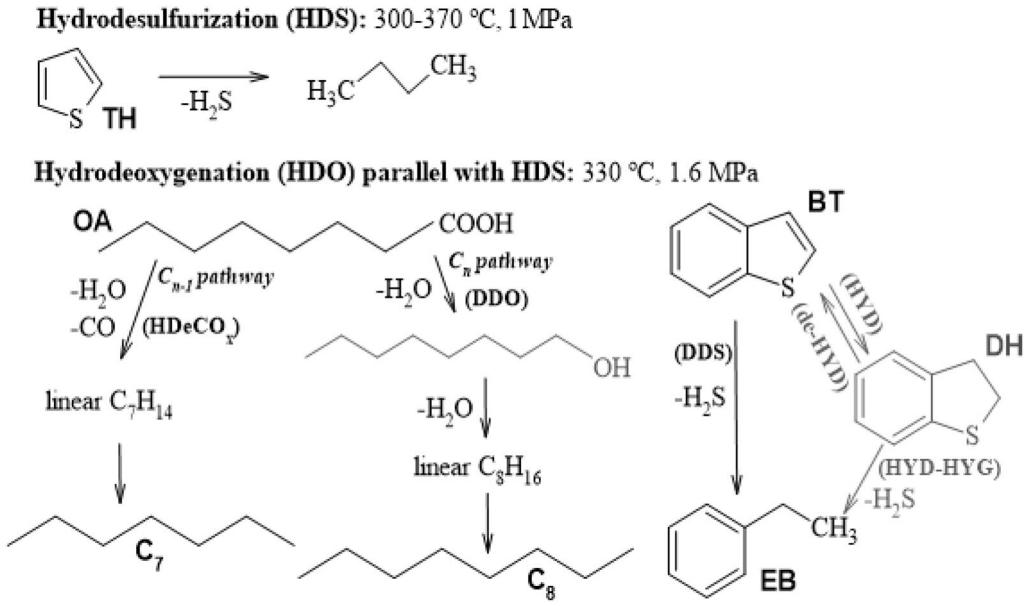

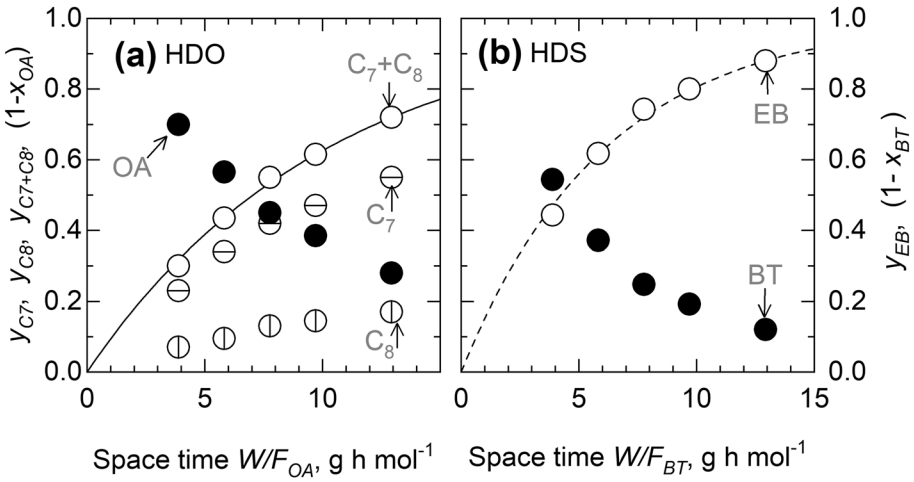

Fig. 7 Example of determination of kHDO (**a**) and kHDS (**b**) activity in parallel HDO/HDS of octanoic acid (OA)/1–benzothiophene (BT) on $NiMo_6$-0.1 catalyst: Solid line—fitting of pseudo-first order rate constant kHDO, Eq. (2); dash line—fitting of pseudo–first order rate constant kHDS, Eq. (3); **a** C_7—linear C_7 hydrocarbons; C_8—linear C_8 hydrocarbons; C_7+C_8—sum of yields of linear C_7 and C_8 hydrocarbons yC_7+C_8. **b** Relative content of BT ($1–x_{BT}$) and relative yields of ethylbenzene (EB) y_{EB}

Table 7 Results of HDS of thiophene at 340 °C, 1.0 MPa and parallel HDO/HDS of octanoic acid and 1–benzothiophene at 330 °C, 1.6 MPa

Sample	Thiophene HDS	Parallel HDO/HDS				
	Activity	Activity		Selectivity to linear hydrocarbons		Selectivity to HDO
	k_{Th}	k_{HDO}	k_{HDS}	C_7 (HDeCOx)	C_8 (DDO)	HDO/(HDO + HDS)
	$mmol_{(TH)}\ g^{-1}\ h^{-1}$	$mmol_{(C7+C8)}\ g^{-1}\ h^{-1}$	$mmol_{(EB)}\ g^{-1}\ h^{-1}$	y_{C7} at $y_{(C7+C8)}=1$	y_{C8} at $y_{(C7+C8)}=1$	$k_{HDO}/(k_{HDO}+k_{HDS})$
$NiMo_6$-0	102	81	133	0.71	0.29	0.38
$NiMo_6$-0.1	101	98	164	0.74	0.26	0.37
$NiMo_6$-0.2	87	91	185	0.74	0.26	0.33
$NiMo_6$-0.9	39	86	78	0.70	0.30	0.52
$NiMo_6$-1.3	12	49	37	0.69	0.31	0.57

k_{Th} pseudo-first order rate constant calculated by Eq. (1) from thiophene conversion

k_{HDO} total HDO activity obtained by non–linear fitting of C_7+C_8 yields using Eq. (2)

k_{HDS} HDS activity obtained by non–linear fitting of ethylbenzene yields using Eq. (3)

The overall activity of the catalysts was expressed using pseudo-first order rate constants of hydrocarbon formation. The sum of linear C_7+C_8 hydrocarbons formed from octanoic acid was used to calculate the total activity of HDO, k_{HDO}, and the formation of ethylbenzene from 1–benzothiophene was used to calculate the activity of HDS, k_{HDS}. An example how k_{HDO} and k_{HDS} were obtained is shown in Fig. 7. The overview of k_{HDO} and k_{HDS} fitting is given in Fig. S.3 in the Supplementary Information. The activities of catalysts are summarized in Table 7. The highest activity in the parallel HDO reaction was exhibited by the NiMo6-0.1 catalyst with ca. 0.1 wt.% Li ($k_{HDO}=98$ $mmol_{(C7+C8)}$ g_{cat}^{-1} h^{-1}). A slightly higher Li concentration (0.18 wt.%) in the $NiMo_6$-0.2 catalyst reduced the total HDO activity to 91 $mmol_{(C7+C8)}$ g_{cat}^{-1} h^{-1}.

Catalysts with lower and higher lithium contents than the above values showed lower activities. In contrast to the HDO reaction, the parallel HDS of 1–benzothiophene was fastest with a catalyst containing slightly more Li (0.18 wt.%). The 1.3 wt.% lithium content in the catalyst caused a decrease in the overall HDO activity by almost a factor of two and in the case of HDS by almost a factor of five. The findings show that the decrease in surface acidity caused by the introduction of lithium into $NiMo_6$-x catalysts affected the HDS reaction significantly more than HDO.

3.3 Selectivity of the Catalysts

3.3.1 HDO/HDS Selectivity of the Catalysts

HDO/HDS selectivity was expressed as the ratio of k_{HDO} to the sum of k_{HDO} and k_{HDS} (Table 7). The investigated catalysts can be divided into two groups. Modification of $NiMo_6$ catalyst with 0.09 and 0.18 wt.% lithium caused a slight decrease in HDO/HDS selectivity from 0.38 to approximately 0.33. A second group of catalysts with higher Li content exhibited HDO/HDS selectivities higher than 0.51. This represents a more than 1.34-fold increase in the HDO/HDS selectivity index compared to the first group. It is evident that Li content in NiMo catalysts higher than 0.9 wt.% decreased HDS activity more than HDO activity.

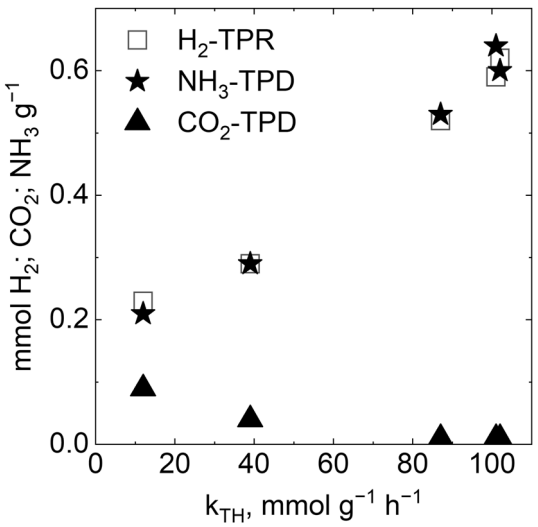

Fig. 8 Relationship between H_2 consumption determined by TPR measurements, the amount of desorbed NH_3 and CO_2 determined during TPD experiments (per gram of Li-modified $NiMo_6$-x catalysts, temperature range 25–500 °C) and the rate constant k_{Th}

3.3.2 Selectivity to Reaction Intermediates During HDO/HDS

Regarding the selectivity towards the reaction intermediates in the HDO/HDS reactions of octanoic acid and 1–benzothiophene, i.e., octanol, the reaction intermediate of direct deoxygenation of octanoic acid, and dihydrobenzothiophene, the reaction intermediate of 1–benzothiophene hydrodesulfurization, this selectivity was similar and negligible over all prepared catalysts. The relative content of octanol and dihydrobenzothiophene in the reaction mixtures hardly reached the value of 0.01. These relative contents did not change with increasing Li concentration in the catalysts. Therefore, these intermediates were not discussed in schemes (5–10) and Fig. 8.

Similarly, no cracking activity was observed for the catalysts (C_{7-x} pathway). Branched hydrocarbons, such as 2-methyl-hexane, 3-methyl-hexane, 2-(or 4)methyl-heptane, and 3-methyl-heptane, were only observed in low yields (less than 1% of C_8+C_7 yields) and were, therefore, not discussed. In contrast, the selectivity towards linear C_7 and C_8 hydrocarbons during HDO of octanoic acid was clearly expressed.

For all catalysts, the C_7 pathway (dehydration decarbonylation/decarboxylation, $HDeCO_x$) predominated, yielding C_7 olefins and finally n-heptane according to Eqs. (6, 7, 8). All catalysts showed similar selectivities for C_7 hydrocarbons, approximately 69–74% of the total hydrocarbons yields listed in Table 7. The C_8 pathway (direct hydrodeoxygenation, DDO) with yields of C_8 olefins and finally n-octane according to Eqs. (9, 10) was less pronounced. The formation of linear olefins, intermediates of the HDO reaction, was observed at low space time, while hydrogenation to both n-octane and n-heptane was predominant at higher space time. An example of a simplified reaction progress kinetic analysis (RPKA), i.e., an example of the formation of linear olefins and linear alkanes in HDO, is given in the Supplementary Information (Fig. S.4). The same progression was observed in our previous work on NiMo sulfides on commercial supports [27].

4 Discussion

NiMo catalysts prepared from the ammonium salt of Ni Anderson–type polyoxomolybdate over γ–alumina were modified by small amounts of lithium to obtain catalysts with different acid–base properties of the catalyst surface. A relatively small amount of lithium (less than 1 wt.%) added to molybdonickelate slightly reduced the surface area (by about 10 rel. %). However, a higher amount of Li (1.3 wt.%) in the catalyst surprisingly increased the surface area, very likely, due to the partial decomposition of molybdonickelate during the impregnation of Ni/Al_2O_3 particles and probably the formation of Li-molybdates and/or Ni–O (Li–O-Ni) species as shown by FTIR (Fig. 3). The mesopore volume and other pore characteristics changed only to a limited extent.

Temperature-programmed NH_3 desorption revealed the dependence of the amount and strength of acid sites on the addition of Li. A very low concentration of Li (about 1 wt.%) added to the $NiMo_6$-x catalysts prepared from Ni Anderson salt substantially affected their acidity. The acidity (expressed in mmol NH_3 g^{-1} desorbed between 25 and 500 °C) of the catalyst with 1.3 wt.% Li dropped to one third of the value found for the unmodified catalyst. The strength of the stronger sites increased slightly as the temperature maxima of desorption shifted to higher temperatures (Fig. 2). The catalyst basicity values confirmed the acidic nature of the POM-prepared catalysts, as the basicity of the Li unmodified catalyst was very low. Basicity was increasing after gradual introduction of an alkali metal, Li, into the catalysts. Basicity of the catalyst with the highest Li concentration differed significantly from the other catalysts: the temperature maxima of CO_2 desorption was shifted to lower temperatures, indicating a decrease in the strength of the basic sites. With increasing Li concentration in the catalysts, the temperature-programmed H_2-TPR reduction showed a shift of the temperature maxima of metal oxide reduction present in the calcined catalysts to higher temperatures (Fig. 1), probably due to the strong interaction of Li with polymolybdates, both octahedral and tetrahedral, as well as the strong interaction of polyoxometalate with the support surface.

FTIR spectra (Fig. 3) revealed the preservation of the original polyoxometalate (POM) compound structure for samples with low Li concentration (Li < 0.2 wt.%). For samples with higher Li amount (Li concentration > 0.9 wt.%), the pH of the impregnation solution was much higher than that of the solution without Li and the structure of initial Anderson salt used for catalyst preparation was destroyed (characteristic bands at ca. 947 and 1043 cm^{-1} disappeared). In addition, FTIR spectra obtained in the 800–4000 cm^{-1} region showed the presence of crystalline and constitutional water, with larger amounts observed for samples containing 0.9 and 1.3 wt.% Li. It is very likely that the high basicity of the impregnation solution caused by the addition of alkali contributes to the decomposition of the Ni polyoxometalate (POM) and the resulting water is adsorbed on the support. Thus, it can be concluded that, based on the above reasons, it does not make sense to add more than – 0.9 wt.% Li to the catalyst, since the Anderson salt is not stable at pH value higher than 5.

The role of nickel, which is deposited on the support prior to POM impregnation, is also not negligible. Adsorption studies of various Anderson polyoxometalates have indicated that nickel POM exhibits the lowest adsorption strength on alumina [53] and thus more nickel remains on the surface without aluminate formation. It is evident that the nickel initially introduced on the alumina support interacted with the basic OH groups of the support surface and thus reduced the possible decomposition of POM. Therefore, nickel added to the support prior to its impregnation with Anderson salt contributes to the retention of nickel in the position of countercation in the Anderson salt and apparently helps to preserve the structure of the supported POM [45]. Moreover, Ni^{2+} ions present on the alumina surface could interact with the loaded Anderson salt by substituting NH_4^+ ions and lead to a highly dispersed, easily reducible form of the surface compound. However, H_2-TPR experiments revealed a shift of the temperature reduction maxima to higher values with increasing amounts of lithium in the catalysts. This implies that catalysts with higher Li concentration are not easily

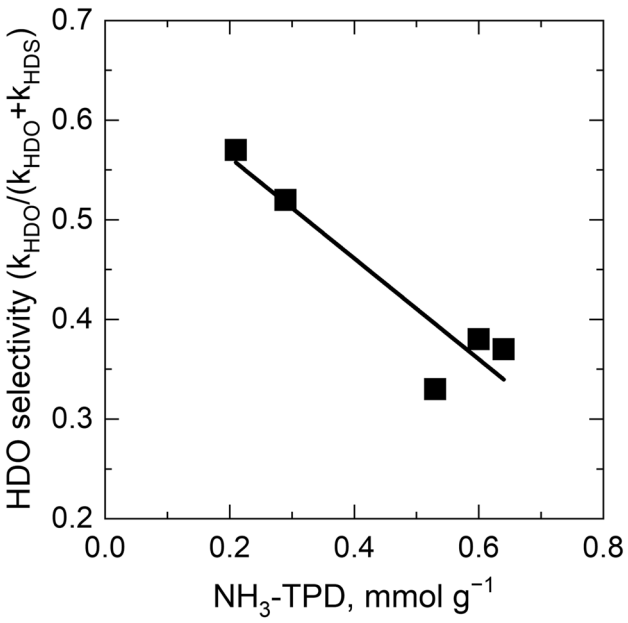

Fig. 9 Dependence of HDO selectivity on acidity (expressed as the amount of desorbed NH_3 in the temperature range 25–500 °C) of $NiMo_6$-x catalysts

reducible and therefore their hydrogenation function would be worse. These findings may affect the ability of the catalysts in the HDO/HDS reaction.

Findings in literature [14] inform that O- and S-containing compounds compete for the same active sites of hydrotreatment catalysts. The catalysts synthesized using $(NH_4)_4Ni(OH)_6Mo_6O_{18}$ Anderson salt and Li_2CO_3 leading to catalysts with various acid–base and reduction properties confirmed their role in hydrodesulfurization reaction and parallel treatment of 1–benzothiophene and octanoic acid. The HDS of thiophene gradually decreased with increasing Li concentration due to decreasing acidity, increasing basicity and decreasing reducibility of the catalysts (Fig. 8, Table 1). It is clear that acidic sites are essential for the activation of thiophene in its HDS reaction.

The situation in parallel HDO/HDS of octanoic acid and 1–benzothiophene is more complex. In these reactions, the selectivity of the catalysts depends on their acidity (Fig. 9), which is determined by the properties of the support, the molybdenum compound added and the lithium concentration (Table 1). The acidity of the catalysts affects the reaction rates of both HDO octanoic acid and 1–benzothiophene HDS, but in different ways. Small amounts of added lithium (0.1 and 0.2 wt.%) increased catalyst activity for HDS 1–benzothiophene by 40%. Similar to the case of HDS thiophene, the HDS of 1–benzothiophene decreased with decreasing catalyst acidity. However, the HDO reaction rate of octanoic acid increased up to a certain acidity value (about 0.5 mmol NH_3 g^{-1}) and then seemed to decrease.

The conversion of octanoic acid, which is a part of the reaction mixture, probably positively influences the conversion of 1–benzothiophene by HDS, since hydrotreatment leads to the formation of H_2O. It is clear that the affinity of lithium for water alters the necessary acid–base properties of the catalysts in the HDO reaction, and these reach an optimum at certain Li concentrations. The HDO activity of octanoic acid on the catalyst prepared from an Anderson salt is increased by 20% if the catalyst contains 0.1 wt.% Li, while at a concentration of 0.18 wt.% Li it increases only by 12%. In the case of HDS of 1–benzothiophene, the activity of the investigated catalysts increased by 20–40%. It is noteworthy that the catalyst with higher Li content shows higher activity.

As for the selectivity of the examined catalysts in HDO reaction is concerned, the C_7 pathway (dehydration decarbonylation/decarboxylation, $HDeCO_x$) yielding first C_7 olefins and finally n-heptane predominated over all catalysts. All catalysts revealed similar selectivity to C_7 hydrocarbons about 70% from the total yield of hydrocarbons. The C_8 pathway (the direct hydrodeoxygenation, HDO) yielding C_8 olefins and finally n-octane was less pronounced. Linear olefins, the intermediates of the HDO reaction, were observed at low space–time, while hydrogenation to n-octane and n-heptane predominated at higher space–time. In HDO/HDS processes, two reactions take place on the catalyst, but probably involving different catalyst centers. Nickel is apparently active in both processes. Nickel enhances the acidity of $NiMo/Al_2O_3$ catalysts [54], forming active sites for HDS reactions together with Mo because of its ability to donate electrons to Mo and thus increase the electron density on Mo [55]. Nickel is also very important for the hydrogenation of octanoic acid. The oxygen-containing reactant can be adsorbed on the catalyst and its O^- ion, as well as H_2O formed during reactant hydrogenation, can decrease the electron density of Mo^{+4} to Mo^{+5}. It is very likely that the low concentration of lithium, which has an affinity to H_2O, helps to create balance between the acidity and reducibility of the catalyst.

As can be seen from the FTIR spectra (Fig. 3), the catalysts $NiMo_6$-0, $NiMo_6$-0.1 and $NiMo_6$-0.2 have a close spectral image with some difference in intensity. The consumption of H_2 (Table 1) taken up to 500 °C decreases from 62 to 52 mmol g^{-1}, indicating that the addition of Li reduces the reduction of molybdenum. Comparison of these data with the activity of the samples during HDS of 1–benzothiophene and HDO of octanoic acid (Table 7) shows that Li at a low concentration of 0.1–0.2 wt.% has a positive effect on these reactions. It can be assumed that the situation in these samples is analogous to that observed in our earlier work with $NiMo_6$-based catalysts [56].

It has been shown that the presence of certain amount of MoO_xS_y, originated from tetrahedral MoO_4^{2-} species, is beneficial for high HDS activity. Nevertheless, MoO_xS_y phase exist in all prepared catalysts (Table 6). Thus, the low loading of Li has to interact also in other way. Lithium in the presence of octanoic acid contributes to the formation of other portion of the active phase, thus achieving higher activity of Li-modified samples in HDO/HDS reactions. It is clear from the experimental XPS data that maximum synergy exists between the $MoS_2(MoO_xS_y)$ and NiS_x phases at low Li content. In the case of a catalyst containing a high concentration of Li, the high basicity of the catalyst prevails over the positive effect caused by the interaction between lithium and octanoic acid, and therefore the resulting activity in the HDO/HDS reaction is low.

The presented data obtained from HDS of thiophene in the presence of Li-modified $NiMo/Al_2O_3$ catalysts did not confirm the expected improvement in catalyst activity previously observed for $NiMo/SiO_2$ catalysts [9]. This finding can be explained by the ability of the unmodified alumina support to provide a sufficiently high dispersion of molybdenum. However, the addition of lithium to the alumina-supported catalysts gradually decreased their acidity and, for this reason, reduced their activity in HDS of thiophene.

5 Conclusions

Parallel processing of octanoic acid and 1-benzothiophene in HDO and HDS hydroprocessing showed relatively high activity of the catalyst containing $(NH_4)_4NiMo_6O_{24}H_6$ Anderson salt in both reactions. The low amount of lithium added to the catalyst (0.1–0.2 wt.%) did not cause significant changes in the acid–base properties of the catalysts. However, this low amount of lithium significantly increased the activity during the hydrotreatment of the mixed feedstock, in HDS by 40% in the case of 1-benzothiophene, and in HDO by 18% in the case of octanoic acid. The interaction of octanoic acid with these low amounts of Li thus created additional active centers for the HDO/HDS reactions. Such centers were not present in the HDS of thiophene. In contrast, the high amount of lithium added to the catalysts (0.9–1.3 wt.%) had detrimental effect on the studied acid–base properties and HDS and HDO/HDS activities.

The optimization of the catalyst preparation, i.e., the selection of a support with the necessary acid–base properties, a suitable heteropolycompound and its modification procedure can obviously lead to high catalyst activity in the hydrogenation of mixed feedstocks.

Supplementary Information The online version contains supplementary material available at https://doi.org/10.1007/s10562-023-04315-0.

Acknowledgements The authors thank Ms. Hana Šnajdaufová for the characterization of porous structure of catalysts. The authors are grateful for the support of the mobility project of the Czech and Bulgarian Academies of Sciences (Project Nos. BAS-20-01 and BAS-23-01).

Funding This study is supported by the mobility project of the Czech and Bulgarian Academies of Sciences (Project Nos. BAS-20-01 and BAS-23-01).

Data Availability The data will be made available on request.

Declarations

Conflict of interest The authors declare that they have no known competing financial interests or personal relationships that could have appeared to influence the work reported in this article.

References

1. K.Y. Lee, M. Misono (1997) in: Handbook of heterogeneous catalysis, vol. 1, eds. G. Ertl and H. Knoezinger. Wiley–VCH, Weinheim.
2. Hayashi H, Moffat JB (1983) Methanol conversion over metal salts of 12-tungstophosphoric acid. J Catal 81:61–66. https://doi.org/10.1016/0021-9517(83)90146-X
3. Misono M (1987) Heterogeneous catalysis by heteropoly compounds of molybdenum and tungsten. Catal Rev-Sci Eng 29:269–321. https://doi.org/10.1080/01614948708078072
4. Cheng WC, Luthra NP (1988) NMR study of the adsorption of phosphomolybdates on alumina. J Catal 109:163–169. https://doi.org/10.1016/0021-9517(88)90194-7
5. Goncharova OI, Yurieva TM, Davydov AA (1985) Influence of the nature of the support on the composition and structure of molybdenum supported heteropolycompounds. Kinet Catal (Transl of Kinet Katal) 27:942–949
6. Palcheva R, Spojakina AA, Dimitrov L, Jiratova K (2009) 12-Tungstophosphoric heteropolyacid supported on modified SBA-15 as catalyst in HDS of thiophene. Micropor Mesopor Mater 122(1–3):128–134. https://doi.org/10.1016/j.micromeso.2009.02.026
7. Kraleva E, Spojakina AA, Edreva-Kardjieva R, Jiratova K, Petrov L (2007) Titania-supported mixed HPMoV polyoxometallates as precursors of hydrodesulfurization catalysts. React Kinet Catal Lett 92(1):111–119. https://doi.org/10.1007/s11144-007-4896-8
8. Spojakina A (1994) Damyanova S (1994) IR and DRS study of TiO_2-supported 12-molybdophosphoric heteropolycompounds. React Kinet Catal Lett 53(2):405–412. https://doi.org/10.1007/BF02073049
9. Spojakina A, Kostova N, Jiratova K (1998) Effect of heteroatom on properties of SiO_2-supported heteropolymolybdates. Collect Czech Chem Commun 63:1927. https://doi.org/10.1135/cccc19981927
10. Spojakina A, Jiratova K, Kostova N, Kocianova J, Stamenova M (2003) Tungsten/alumina catalysts: effect of $H_3PW_{12}O_{40}$ countercation on surface properties and hydrodesulfurization activity. Kinet Katal 44:813–818. https://doi.org/10.1023/B:KICA.0000009059.80675.4e
11. van Veen JAR, Hendriks PAJM, Andrea RR, Romers EJGM, Wilson AE (1990) Chemistry of phosphomolybdate adsorption on alumina surfaces 1: the molybdate/alumina system. J Phys Chem 94:5275–5282. https://doi.org/10.1021/j100376a021
12. Nikulshin PA, Mozhaev AV, Pimerzin AA, Konovalov VV, Pimerzin AA (2012) CoMo/Al_2O_3 catalysts prepared on the basis of Co_2Mo_{10}-heteropolyacid and cobalt citrate: effect of Co/Mo ratio. Fuel 100:24–33. https://doi.org/10.1016/j.fuel.2011.11.028
13. Cabello CI, Cabrerizo FM, Alvarez A, Thomas HJ (2002) Decamolybdodicobaltate(III) heteropolyanion: structural, spectroscopical, thermal and hydrotreating catalytic properties. J Mol Catal A: Chem 186:89–100. https://doi.org/10.1016/S1381-1169(02)00043-2
14. Nikulshin PA, Mozhaev AV, Ishutenko DI, Minaev PP, Lyashenko AI, Pimerzin AA (2012) Influence of the composition and morphology of nanosized transition metal sulfides prepared using the Anderson-type heteropoly compounds $[X(OH)_6Mo_6O_{18}]n-$ (X = Co, Ni, Mn, Zn) and $[Co_2Mo_{10}O_{38}H_4]^{6-}$ on their catalytic properties. Kinet Catal 53:620–631. https://doi.org/10.1134/S0023158412050114
15. Pimerzin AA, Tomina NN, Nikulshin PA et al (2015) Catalysts based on molybdenum and tungsten heteropoly compounds for the hydrotreatment of oil fractions. Catal Ind 7:30–37. https://doi.org/10.1134/S2070050415010110
16. Dhandapani B, Clair TSt, Oyama ST (1998) Simultaneous hydrodesulfurization, hydrodeoxygenation, and hydrogenation with molybdenum carbide. Appl Catal A 168:219–228. https://doi.org/10.1016/S0926-860X(97)00342-6
17. Odebunmi EO, Ollis DF (1983) Catalytic hydrodeoxygenation II: interactions between catalytic hydrodeoxygenation of m-cresol and hydrodesulfurization of benzothiophene and dibenzothiophene. J Catal 80:65–75. https://doi.org/10.1016/0021-9517(83)90230-0
18. Varakin AN, Salnikov VA, Nikulshina MS, Maslakov KI, Mozhaev AV, Nikulshin PA (2017) Beneficial role of carbon in Co(Ni)MoS catalysts supported on carbon-coated alumina for

co-hydrotreating of sunflower oil with straight-run gas oil. Catal Today 292:110–120. https://doi.org/10.1016/j.cattod.2016.10.031
19. Vonortas A, Papayannakos N (2016) Hydrodesulphurization and hydrodeoxygenation of gasoil-vegetable oil mixtures over a Pt/γ-Al2O3 catalyst. Fuel Process Technol 150:26–131. https://doi.org/10.1016/j.fuproc.2016.05.013
20. Vonortas A, Kubicka D, Papayannakos N (2014) Catalytic co-hydroprocessing of gasoil–palm oil/AVO mixtures over a NiMo/γ-Al2O3 catalyst. Fuel 116:49–55. https://doi.org/10.1016/j.fuel.2013.07.074
21. Nikulshin PA, Salnikov VA, Pimerzin AA et al (2016) Co-hydrotreating of straight_run diesel fraction and vegetable oil on Co(Ni)-PMo/Al2O3 catalysts. Petrol Chem 56:56–61. https://doi.org/10.1134/S0965544115080150
22. Kaluža L, Zdražil M, Gulková D, Vít Z (2013) The influence of the chelating agent nitrilotriacetic acid on promotion of hydrodesulfurization activity by Co in CoMo catalysts prepared on Al_2O_3, C, and ZrO_2 supports. Chem Eng Trans 32:841–846. https://doi.org/10.3303/CET1332141
23. Kaluža L, Gulková D, Vít Z, Zdražil M (2007) Effect of support type on the magnitude of synergism and promotion in CoMo sulphide hydrodesulphurisation catalyst. Appl Catal A Gen 324:30–35. https://doi.org/10.1016/j.apcata.2007.02.050
24. Furimsky E (2000) Catalytic hydrodeoxygenation. Appl Catal A 199:147–190. https://doi.org/10.1016/S0926-860X(99)00555-4
25. Mortensen PM, Grunwaldt JD, Jensen PA, Knudsen KG, Jensen AD (2011) A review of catalytic upgrading of bio-oil to engine fuels. Appl Catal A 407:1–19. https://doi.org/10.1016/j.apcata.2011.08.046
26. Furimsky E (2013) Hydroprocessing challenges in biofuels production. Catal Today 217:13–56. https://doi.org/10.1016/j.cattod.2012.11.008
27. Kaluža L, Karban J, Gulková D (2013) Activity and selectivity of Co(Ni)Mo sulfides supported on MgO, Al2O3, ZrO2, TiO2, MCM-41 and activated carbon in parallel hydrodeoxygenation of octanoic acid and hydrodesulfurization of 1-benzothiophene. React Kinet Mech Catal 127:887–902. https://doi.org/10.1007/s11144-019-01620-x
28. Varakin AN, Mozhaev AV, Pimerzin AA, Nikulshin PA (2020) Toward HYD/DEC selectivity control in hydrodeoxygenation over supported and unsupported Co(Ni)-MoS_2 catalysts. A key to effective dual-bed catalyst reactor for co-hydroprocessing of diesel and vegetable oil. Catal Today 357:556–564. https://doi.org/10.1016/j.cattod.2019.06.005
29. Ramesh A, Tamizhdurai P, Krishnan PS, Ponnusamy VK, Sakthinathan S, Shanthi K (2020) Catalytic transformation of non-edible oils to biofuels through hydrodeoxygenation using Mo-Ni/mesoporous alumina-silica catalysts. Fuel 262:116494. https://doi.org/10.1016/j.fuel.2019.116494
30. Solís-Casados DA, Escobar-Alarcón L, Klimova T et al (2016) Catalytic performance of CoMo/Al_2O_3-MgO-Li(x) formulations in DBT hydrodesulfurization. Catal Today 271:35–44. https://doi.org/10.1016/j.cattod.2015.07.046
31. Escobar-Alarcyn L, Klimova T, Escobar-Aguilar J, Romero S, Morales-Ramirez C, Solis-Casados D (2013) Preparation and characterization of Al_2O_3–MgO catalytic supports modified with lithium. Fuel 110:278–285. https://doi.org/10.1016/j.fuel.2012.10.013
32. Tsigdinos GA (1978) Heteropoly compounds of molybdenum and tungsten. Top Curr Chem 76:1–64. https://doi.org/10.1007/BFb0047026
33. Brunauer S, Emmett PH, Teller E (1938) Adsorption of gases in multimolecular layers. J Am Chem Soc 60:309–319. https://doi.org/10.1021/ja01269a023
34. Barrett EP, Joyner LG, Halenda PP (1951) the determination of pore volume and area distributions in porous substances I: computations from nitrogen isotherms. J Am Chem Soc 73:373–380. https://doi.org/10.1021/ja01145a126
35. Lecloux A, Pirard JP (1979) The importance of standard isotherms in the analysis of adsorption isotherms for determining the porous texture of solids. J Colloid Interface Sci 70:265–281. https://doi.org/10.1016/0021-9797(79)90031-6
36. Glotov AP, Vutolkina AV, Vinogradov NA, Pimerzin AA, Vinokurov VA, AlA P (2021) Enhanced HDS and HYD activity of sulfide Co-PMo catalyst supported on alumina and structured mesoporous silica composite. Catal Today 377:82–91. https://doi.org/10.1016/j.cattod.2020.10.010
37. Lan X, Pestman R, Hensen EJM, Weber T (2021) Furfural hydrodeoxygenation (HDO) over silica-supported metal phosphides – The influence of metal–phosphorus stoichiometry on catalytic properties. J Catal 403:181–193. https://doi.org/10.1016/j.jcat.2021.01.031
38. Wu H, Duan A, Zhao Z, Li T, Prins R, Zhou X (2014) Synthesis of NiMo hydrodesulfurization catalyst supported on a composite of nano-sized ZSM-5 zeolite enwrapped with mesoporous KIT-6 material and its high isomerization selectivity. J Catal 317:303–317. https://doi.org/10.1016/j.jcat.2014.07.002
39. Davydov AA, Goncharova OI (1993) Use of IR spectroscopy in studies of catalysts based on molybdenum heteropoly compounds supported on oxides. Usp Khim 62:118–134. https://doi.org/10.1070/RC1993v062n02ABEH000008
40. Scofield JH (1976) Hartree-Slater subshell photoionization cross-sections at 1254 and 1487 eV. J Electron Spectrosc Relat Phenomena 8:129–137. https://doi.org/10.1016/0368-2048(76)80015-1
41. Vissers JPR, Scheffer B, de Beer VHJ, Moulijn JA et al (1987) Effect of the support on the structure of Mo-based hydrodesulfurization catalysts: activated carbon versus alumina. J Catal 105:277–284. https://doi.org/10.1016/0021-9517(87)90058-3
42. Kordulis CH, Voliotis S, Lycourghiotis A, Vattis D, Delmon B (1984) Studies on the state of dispersion of Mo(VI) supported on γ-Al_2O_3 doped with alkali cations. Appl Catal 11:179–193. https://doi.org/10.1016/S0166-9834(00)81877-1
43. Cabello CI, Botto IL, Thomas HJ (1994) Reducibility and thermal behavior of some Anderson phases. Thermochim Acta 232:183–193. https://doi.org/10.1016/0040-6031(94)80058-8
44. Tanabe K, Makoto M, Ono Y, Hattori, H (1989) New solid acids and bases. Stud Surf Sci Catal 51, 1st ed., Elsevier, Kodansha.
45. Palcheva R, Kaluža L, Spojakina A, Jirátová K, Tyuliev G (2012) NiMo/γ-Al2O3 catalysts from Ni heteropolyoxomolybdate and effect of alumina modification by B Co, or Ni. Chin J Catal 33:952–961. https://doi.org/10.1016/S1872-2067(11)60376-8
46. Nikulshin PA, Tomina NN, Pimerzin AA, Stakheev AYu, Mashkovsky IS, Kogan, (2011) Effect of the second metal of Anderson type heteropolycompounds on hydrogenation and hydrodesulphurization properties of XMo6(S)/Al2O3 and Ni3-XMo6(S)/Al2O3 catalysts. Appl Catal A: Gen 393:146–152. https://doi.org/10.1016/j.apcata.2010.11.033
47. Nicosia D, Prins R (2005) 31P MAS NMR and Raman study of a Co(Zn)MoP/γ -Al2O3 HDS catalyst precursor containing triethylene glycol. J Catal 234:414–420. https://doi.org/10.1016/j.jcat.2005.07.011
48. Escobar J, Barrera MC, Gutiérrez AW, Cortés-Jacome MA, Angeles-Chávez C, Toledo JA, Solís-Casados DA (2018) Highly active P-doped sulfided NiMo/alumina HDS catalysts from Mo-blue by using saccharose as reducing agents precursor. Appl Catal B-Environ 237:708–720. https://doi.org/10.1016/j.apcatb.2018.06.034
49. Nyquist RA, Nagel RO (1971) Infrared spectra of inorganic compounds. Academic Press, New York

50. Bielanski A, Malecka A, Kubelkova, (1989) Infrared study of the thermal decomposition of heteropolyacids of the series $H_{3+x}PMo_{12-x}V_xO_{40}$. J Chem Soc Faraday Trans 1(85):2847–2856. https://doi.org/10.1039/F19898502847
51. Mansour AN (1994) Characterization of $LiNiO_2$ by XPS. Surf Sci Spectra 3:279–286. https://doi.org/10.1116/1.1247757
52. Jichang Lu, Luo Y, He D et al (2020) An exploration into potassium containing MoS2 active phases and its transformation process over MoS2 based materials for producing methanethiol. Catal Today 339:93–104. https://doi.org/10.1016/j.cattod.2019.01.012
53. Cabello CI, Botto IL, Gabriezo F, Gonzales MG, Thomas HJ (2000) γ-Al_2O_3-supported XMo_6 Anderson heteropolyoxomolybdates: adsorption studies for X = TeVI, AlIII, CoIII, CrIII and NiII by DR spectroscopy and TPR analysis. Ads Sci Technol 18:591–608. https://doi.org/10.1260/0263617001493657
54. Baba T, Watanabe E, Ono Y (1983) Generation of acidic sites in metal salts of heteropoly acids. J Phys Chem 87:2406–2411. https://doi.org/10.1021/j100236a033
55. Harris S, Chianelli RR (1986) Catalysis by transition metal sulfides: a theoretical and experimental study of the relation between the synergic systems and the binary transition metal sulfides. J Catal 98:17–31. https://doi.org/10.1016/0021-9517(86)90292-7
56. Kaluža L, Jirátová K, Tyuliev G et al (2018) Hydrodesulfurization NiMo catalysts over gamma-alumina prepared mechanochemically. React Kinet Mech Catal 125:319–337. https://doi.org/10.1007/s11144-018-1436-7